Sensitivity of the representation of polar lows to typical climate model resolutions

Moreno-Ibáñez, M. ORCID: https://orcid.org/0000-0001-5703-4699, Cassano, J. J., Gray, S. L. ORCID: https://orcid.org/0000-0001-8658-362X and Seefeldt, M. (2025) Sensitivity of the representation of polar lows to typical climate model resolutions. Atmospheric Science Letters, 26 (9). e1319. ISSN 1530-261X doi: 10.1002/asl.1319 Available at https://centaur.reading.ac.uk/124382/

Atmospheric Science Letters

RMetS Royal Meteorological Society

RESEARCH ARTICLE OPEN ACCESS

Sensitivity of the Representation of Polar Lows to Typical Climate Model Resolutions

Marta Moreno-Ibáñez[1,2,3] | John J. Cassano[2,3,4] | Suzanne L. Gray[1] | Mark Seefeldt[2,3]

[1]Department of Meteorology, University of Reading, Reading, UK | [2]Cooperative Institute for Research in Environmental Sciences, University of Colorado Boulder, Boulder, Colorado, USA | [3]National Snow and Ice Data Center, University of Colorado Boulder, Boulder, Colorado, USA | [4]Department of Atmospheric and Oceanic Sciences, University of Colorado Boulder, Boulder, Colorado, USA

Correspondence: Marta Moreno-Ibáñez (m.morenoibanez@pgr.reading.ac.uk)

Received: 12 May 2025 | **Revised:** 18 July 2025 | **Accepted:** 22 August 2025

Funding: Marta Moreno-Ibáñez was supported by the CIRES Visiting Fellows Program, funded by NOAA NA22OAR4320151. John J. Cassano and Mark Seefeldt are supported by the Regional and Global Model Analysis (RGMA) component of the Earth and Environmental System Modeling (EESM) program of the US Department of Energy's Office of Science, as a contribution to the HiLAT-RASM project. This work utilised the Alpine high performance computing resource at the University of Colorado Boulder. Alpine is jointly funded by the University of Colorado Boulder, the University of Colorado Anschutz, Colorado State University and the National Science Foundation (award 2201538). Data storage was supported by the University of Colorado Boulder 'PetaLibrary'. Publication of this article was funded by the University of Reading through an institutional agreement with *Atmospheric Science Letters*. The statements, findings, conclusion and recommendations are those of the authors and do not necessarily reflect the views of NOAA or the US Department of Commerce.

ABSTRACT

Polar lows (PLs) are intense maritime mesoscale cyclones that often form during marine cold air outbreaks. The objective of this study is to determine the atmospheric model horizontal resolution needed to correctly represent PLs for climate modelling. Three simulations have been conducted with the Weather Research and Forecasting (WRF) model using grid spacings of 50, 25 and 12.5 km. PLs have been tracked using a combination of objective and subjective tracking methods. The number of PLs detected in each simulation increases, and their average equivalent radius decreases, as the model resolution increases. A comparison against three PL track climatologies shows that the hit rate increases with increasing resolution of the atmospheric model. The lifetime maxima of the area-maximum 10-m wind speed and area-average surface sensible heat fluxes associated with PLs are on average 12% and 20% larger, respectively, in the higher-resolution simulations than in the lower-resolution one. The lifetime maximum of the area-maximum 1-h accumulated precipitation is 67% and 133% larger in the 25- and 12.5-km simulations, respectively, than in the lower-resolution one. We conclude that a better representation of PLs can be obtained by increasing the resolution of atmospheric models from 50 to 25 km, but further increasing the resolution to 12.5 km will not result in a substantial improvement.

1 | Introduction

Polar lows (PLs) are intense maritime mesoscale cyclones that form poleward of the main polar front (Renfrew 2015). Their diameter ranges from 200 to 1000 km (Turner et al. 2003), and they are associated with near-surface wind speeds exceeding 15 m s^{-1} (Heinemann and Claud 1997). Although their lifetime is usually 3–36 h (Renfrew 2015), some of them have a lifetime exceeding 48 h (Blechschmidt 2008; Rojo et al. 2015). Small-scale, high-frequency atmospheric phenomena such as PLs have an important impact on ocean circulation (Condron et al. 2008). Removing high-frequency atmospheric forcing in simulations with ocean-sea ice models leads to a decrease in the strength of the Atlantic Meridional Overturning Circulation (Jung et al. 2014; Holdsworth and Myers 2015). Condron and Renfrew (2013) found that parameterizing polar mesoscale cyclones, which include PLs,

in a global coupled ocean-sea ice model led to increased depth and frequency of ocean convection. However, the impact of PLs on the ocean is not well understood (Moreno-Ibáñez et al. 2021; Moreno-Ibáñez 2024). Whereas the strong surface heat fluxes associated with PLs lead to sea surface temperature (SST) cooling, upper-ocean mixing processes induced by strong winds lead to SST warming or cooling depending on the temperature profile of the water (Wu 2021). Therefore, some PLs are associated with SST warming (Saetra et al. 2008; Gutjahr and Mehlmann 2024; Tomita and Tanaka 2024), while others are associated with SST cooling (Tomita and Tanaka 2024).

A few studies have analysed how climate change will affect the frequency and spatial distribution of PLs using dynamical downscaling (Zahn and von Storch 2010; Landgren et al. 2019), statistical downscaling (Romero and Emanuel 2017) and a global atmospheric model (Bresson et al. 2022). Long-term studies with global coupled climate models that correctly represent PLs are needed to analyse how PLs are affecting and will affect the ocean circulation under climate change. The potential benefits of using high-resolution coupled climate models to investigate climate change have gained attention in recent years, as shown by the development of the High Resolution Model Intercomparison Project (HighResMIP; Haarsma et al. 2016; Roberts et al. 2025). Case studies have shown that the increase in the horizontal resolution of atmospheric models improves the representation of PLs (e.g., McInnes et al. 2011). Considering multi-event studies, Shkolnik and Efimov (2013) compared the representation of polar mesoscale cyclones in decadal simulations using a global model with a 200-km grid spacing and a regional climate model with 50 and 25 km grid spacings. However, their criteria to identify PLs did not include a marine cold air outbreak (MCAO) criterion and excluded short-lived and very strong PLs. Thus, to the authors' best knowledge, no study has conducted a systematic analysis of the impact of atmospheric model horizontal resolution (typical for climate models) on the representation of PLs developed during a winter season. This study aims at filling in this gap by addressing the following research questions:

1. How does the number and characteristics of PLs represented with a limited-area atmospheric model vary with horizontal resolution?
2. How do the ocean surface heat fluxes associated with PLs vary with horizontal resolution?

2 | Data and Methodology

2.1 | Simulations

Three simulations were conducted with the Advanced Research Weather Research and Forecasting (WRF) Model Version 4.5.1 (Skamarock et al. 2019). WRF is suitable for this study because it has been extensively used to conduct research in mesoscale meteorology (Powers et al. 2017), including research on PLs (e.g., Wu et al. 2011). The vertical grid consists of 40 levels, with the model top at 50 hPa and the domain covers the North Atlantic (Figure 1). The simulations only differ in their grid spacing (50, 25 and 12.5 km), number of horizontal grid points (110 × 90, 220 × 180 and 440 × 360) and time step (4, 2 and 1 min). In what follows, we will refer to the 50, 25 and 12.5-km simulations as W50, W25 and W12.5, respectively.

The same physics schemes were selected for the three simulations (Table 1). This selection was based on previously published studies in applying WRF to the Arctic (Cassano et al. 2011, 2017; Seefeldt et al. 2024). These and other studies (e.g., Hines et al. 2015; Bromwich et al. 2022) have found the greatest sensitivity to the selection of the microphysics, boundary layer and cumulus parameterizations. The other parameterizations have been relatively uniformly applied across WRF simulations of the Arctic. For this study, preliminary simulations were focused on studying the sensitivity of atmospheric simulations to the cumulus parameterization scheme (e.g., Field et al. 2017). Three preliminary one-month simulations of February 2009 with a 50-km grid spacing were conducted using Kain–Fritsch (Kain 2004), Grell-Freitas (Grell and Freitas 2014) and new Tiedtke (Zhang and Wang 2017) cumulus schemes. The simulation output was verified against ERA5 reanalysis (Hersbach et al. 2020) and the Clouds and the Earth's Radiant Energy System Energy Balanced and Filled Level 3b data product (Kato et al. 2018; Loeb et al. 2018). The simulation with the Grell-Freitas cumulus scheme produced too many clouds, and there were not substantial differences between the other two cumulus schemes. Therefore, the Kain–Fritsch scheme was selected. One-month simulations conducted with the 25- and 12.5-km grids showed that the selected physics schemes are also adequate for these resolutions.

The initial conditions and the hourly lateral and ocean surface conditions were provided by ERA5 reanalysis (Hersbach et al. 2020), which has a regular 0.25° latitude-longitude grid with hourly temporal resolution. Spectral nudging of temperature and wind was applied above ~541 hPa. Each simulation was initialised on 1 September 2008 at 0000 UTC and ended on 1 June 2009 at 0000 UTC, and the output frequency was 1 hour. The extended winter season 2008–2009 was selected because of the relatively high number of PLs that developed over the Nordic Seas according to previous climatologies (Noer et al. 2011; Rojo et al. 2015; Smirnova et al. 2015).

2.2 | Detection and Tracking of PLs

PLs were tracked using a combination of objective and subjective tracking methods as described briefly here (details in Appendix S1). First, the sea level pressure (SLP)-based tracking algorithm presented in Crawford et al. (2021) was applied to the hourly SLP field after being adapted to PLs. Second, some PL criteria were applied to determine the tracks that corresponded to potential PLs. Third, the potential PL tracks were manually analysed to determine if they corresponded to PLs. The PL criteria applied are the following:

1. Lifetime $\geq$ 3 h.
2. Equivalent radius $\geq$ 100 km at least once, and never exceeds 500 km.
3. Maximum 10-m wind speed $>$ 15 m s^{-1} at least once.
4. SST-T_{500} $>$ 43 K at least once.

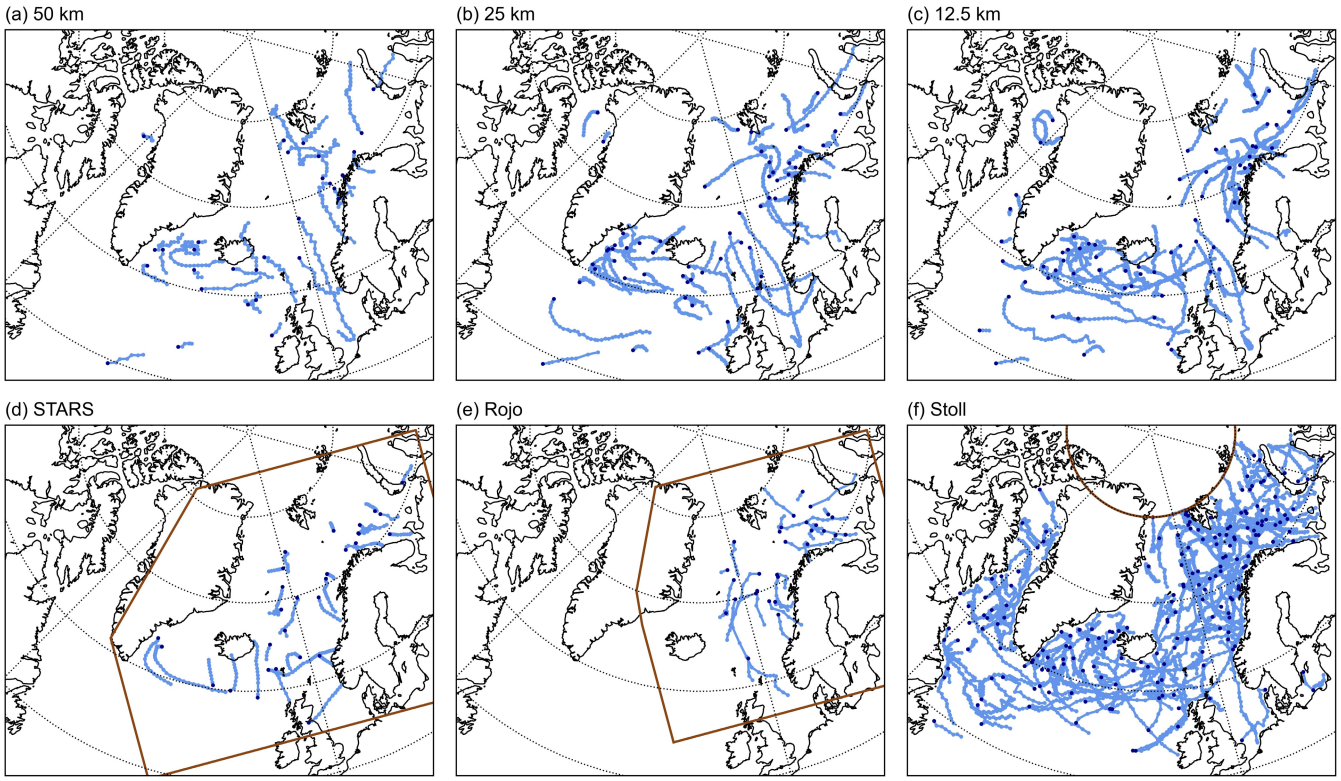

FIGURE 1 | Spatial distribution of PLs in the extended winter season 2008–2009 for the WRF simulations with (a) 50, (b) 25 and (c) 12.5 km resolutions, and for the PL track climatologies of (d) STARS (Noer et al. 2011), (e) Rojo et al. (2015, 2019) and (f) Stoll (2022). Each blue dot represents a track point, and the dark blue dot represents the first track point of each track. The temporal resolution of the track points is 1 h, except for (e), which has a temporal resolution of 3 h since the track points were linearly interpolated to obtain 3-hourly data. The climatologies cover the same period as the WRF simulations. The approximate domains of the STARS and Rojo climatologies, and the domain of the Stoll climatology (between 30° and 80°), are delimited by a brown box.

TABLE 1 | Physics schemes used in the WRF simulations.

Type of scheme	Scheme	References
Radiation—longwave and shortwave	Rapid radiative transfer model for general circulation models (RRTMG)	Iacono et al. (2008)
Planetary boundary layer	Mellor-Yamada-Nakanishi-Niino Level 2.5 (MYNN2)	Nakanishi and Niino (2006) and Nakanishi and Niino (2009)
Microphysics	Morrison two-moment	Morrison et al. (2009)
Deep and shallow convection	Kain–Fritsch scheme	Kain (2004)
Land surface	Unified Noah	Chen and Dudhia (2001) and Tewari et al. (2004)

5. Ocean fraction ≥ 0.75 and sea ice concentration < 0.15 on the first time step of the track.

The values in 4 and 5 are averages within a 100-km radius from the cyclone centre.

2.3 | Analysis of the Characteristics of PLs

Tracking yielded a set of PL tracks with hourly track points for each simulation. The characteristics of each PL track include its lifetime, average equivalent radius, average propagation speed, total distance travelled, and minimum SLP at the PL centre. The average equivalent radius was only computed for PLs that had been assigned a correct (based on visual inspection) equivalent radius by the tracking algorithm more than 50% of their lifetime, which was the case for 90%, 78% and 86% of the PLs in W50, W25 and W12.5, respectively. To compute the average equivalent radius of each PL, track points with an incorrect radius were excluded. In addition, the statistics of certain fields within 200 km from the PL centre were computed: area-maximum 10-m wind speed ($WS10_{max}$), area-maximum 1-h accumulated precipitation ($APCP_{max}$), area-average surface sensible heat fluxes (SHF_{avg}) and area-average surface latent heat fluxes (LHF_{avg}).

TABLE 2 | Number of PLs detected per month and in total for each WRF simulation. Each PL has been assigned to the month when it forms.

Model resolution	Oct 2008	Nov 2008	Dec 2008	Jan 2009	Feb 2009	Mar 2009	Apr 2009	Winter 2008–2009
50 km	7	3	7	8	3	2	0	30
25 km	13	7	9	12	7	8	2	58
12.5 km	10	9	12	17	10	7	1	66

TABLE 3 | Winter 2008–2009 averages of the characteristics of the PLs tracked in the WRF simulations.

	50 km	25 km	12.5 km
Lifetime (h)	24.6	21.8	26.8
Average equivalent radius (km)	197.5	161.4	148.6
Average propagation speed ($m\,s^{-1}$)	8.5	8.1	7.8
Distance travelled (km)	635.0	603.6	731.2
Lifetime minimum sea level pressure at the PL centre (hPa)	982.2	982.1	982.4
Lifetime maximum of the maximum 10-m wind speed within 200 km of the PL centre ($m\,s^{-1}$)	19.7	21.8	22.0
Lifetime maximum of the maximum 1-h accumulated precipitation within 200 km of the PL centre (mm)	2.4	4.0	5.6
Lifetime maximum of the average surface sensible heat fluxes within 200 km of the PL centre ($W\,m^{-2}$)	96.7	116.5	115.6
Lifetime maximum of the average surface latent heat fluxes within 200 km of the PL centre ($W\,m^{-2}$)	131.8	147.7	143.3

The radius selected for the computation of the statistics is similar to or larger than the winter average of the average equivalent radius of the PLs in the WRF simulations (Section 3.1). To compare the characteristics of the PL tracks between each pair of simulations, statistical significance testing using two-tailed permutation tests was performed to test for the differences between the winter averages. The track matching method developed by Crawford et al. (2021) was applied to pairs of datasets of PL tracks using thresholds adjusted for PLs. To be a potential match, two tracks had to be present in at least 50% of their combined observation times, and the average distance between the tracks at the times they overlapped had to not exceed 250 km. From all tracks in the second simulation that fulfilled these two criteria, the one with the smallest average distance was selected as the match for the track in the first simulation. Finally, the PL tracks in each simulation were compared against three PL track climatologies that cover the period and the domain of interest (Figure 1): the Sea Surface Temperature and Altimeter Synergy for Improved Forecasting of Polar Lows (STARS) dataset (Noer et al. 2011), the Rojo dataset (Rojo et al. 2015, 2019) and the dataset of Stoll (2022). Given that the WRF domain is larger than the region covered by the STARS and Rojo datasets, only the tracks whose first track point is within the domain of the relevant climatology are considered for track matching. After experimentation, it was decided to loosen the track matching criteria slightly to increase the number of matches. We selected 40% for the time overlap criterion and 300 km for the distance criterion. In cases where more than one track of the climatology had the same WRF track as a potential match, only one match was counted.

3 | Results

3.1 | Characteristics of PL Tracks in the Simulations

Table 2 shows the temporal distribution of PLs in each simulation. The most PLs during the winter season 2008–2009 are found in W12.5 (66) and W25 (58), whereas the number of PLs in W50 (30) is much lower. Therefore, the number of PLs identified increases as the model resolution increases. PLs occur from October to April, and no PLs were found in any simulation in September and May. This seasonality agrees with climatologies of PLs in the Nordic Seas, which have found that PLs mainly develop from October to April and that it is rare for PLs to develop in September and May (Noer et al. 2011; Rojo et al. 2015). January is the month with the most PLs in W50 and W12.5, and with the second highest number of PLs in W25, consistent with January usually being a month with high PL activity in the Nordic Seas (e.g., Bracegirdle and Gray 2008). The spatial distribution of PLs during the winter season 2008–2009 is shown in Figure 1a–c. In W50, PLs predominantly develop over the Irminger Sea and the Norwegian Sea. In W25 and W12.5, PLs mainly form in the Irminger Sea, the Norwegian Sea and the Barents Sea, in agreement with the high density of PLs found in these regions in PL climatologies (e.g., Stoll 2022). Whereas some PLs form in the Labrador Sea in W12.5, no PLs form over that region in the other simulations. The lack of PLs over the Labrador Sea may be explained by some potential PLs being discarded because their SLP field was affected by the high orography of Greenland (Appendix S1).

The winter averages of the characteristics of PLs are shown in Table 3 (monthly averages are shown in Table S1), and the *p* values are shown in Table S2. Distributions are shown for a subset of these characteristics in Figure 2. Average wintertime PL lifetimes range from 21.8 to 26.8 h. In contrast, subjective climatologies have found an average PL lifetime of 15 h in the Nordic Seas (Smirnova et al. 2015) and 20 h in the North Atlantic (Golubkin

et al. 2021). The longer lifetimes in the simulations are likely explained by the fact that Smirnova et al. (2015) and Golubkin et al. (2021) used satellite observations, which have limited temporal resolution. Most PLs in W50 (63%) and W25 (66%) have a lifetime shorter than 24 h (Figure 2a), consistent with the subjective climatology of Rojo et al. (2015), who found that 67% of PLs lasted less than 24 h. The maximum lifetimes in W50, W25 and W12.5, are 102, 65 and 93 h, respectively; these values are within the range of observed PL lifetimes (e.g., Golubkin et al. 2021). The winter-average of the average equivalent radius decreases as the resolution of the model increases, and the differences are statistically significant at the 1% level when comparing W12.5 and W50, and at the 10% level when comparing W25 and W50. The winter-average of the average equivalent radius in W12.5 is ~149 km, which is the average PL radius estimated by Smirnova et al. (2015). Whereas 80% and 84% of PLs in W25 and W12.5, respectively, have a radius that does not exceed 200 km, the corresponding percentage is 44% in W50 (Figure 2b). The winter-average of the PL average propagation speed ranges from 7.8 to 8.5 $m\,s^{-1}$, consistent with PL climatologies in the North Atlantic (Golubkin et al. 2021) and in the Nordic Seas (Rojo et al. 2015; Smirnova et al. 2015) that found a PL average propagation speed ranging from 8.1 to 8.9 $m\,s^{-1}$. The average distances travelled range from 603.6 to 731.2 km, whereas PL climatologies have found an average of 284 km (Smirnova et al. 2015) and 587 km (Golubkin et al. 2021). None of the differences between the winter means of lifetime, average propagation speed and distance travelled between any pair of simulations is statistically significant.

The winter-average of the minimum SLP at the PL centre is remarkably similar in all simulations. The differences between PLs across simulations are unveiled when analysing their intensity in terms of wind speed and precipitation. The winter-average of the lifetime maximum of $WS10_{max}$ is ~22 $m\,s^{-1}$ in W25 and W12.5, which is ~2 $m\,s^{-1}$ higher than that in W50. These differences are statistically significant at the 1% level. As a comparison, PL climatologies have found an average lifetime maximum of $WS10_{max}$ of ~20 $m\,s^{-1}$ (Smirnova et al. 2015; Golubkin et al. 2021). Only 30% of PLs in W50 show a lifetime maximum of $WS10_{max}$ of at least 21 $m\,s^{-1}$, whereas in W25 and W12.5 the corresponding percentage is 53% and 55%, respectively (Figure 2c). The winter-average of the lifetime maximum of $APCP_{max}$ increases as the resolution increases, and the differences are statistically significant at the 1% level. Whereas 93% of PLs in W50 are associated with a lifetime maximum of $APCP_{max}$ below 4 mm, 79% of PLs in W12.5 are associated with a lifetime maximum of $APCP_{max}$ over 4 mm (Figure 2d). These results show that PL hazard, in terms of high wind speeds and heavy precipitation, is higher in the higher-resolution simulations.

Given that surface heat fluxes depend on near-surface wind speeds, SHF and LHF associated with PLs are expected to be smaller in W50 compared to W25 and W12.5. Indeed, the winter-average of the lifetime maximum of SHF_{avg} is ~19 $W\,m^{-2}$ higher in W25 and W12.5 compared to W50, and these differences are statistically significant at the 10% level. Only 10% of PLs in W50 are associated with a lifetime maximum of SHF_{avg} of at least 150 $W\,m^{-2}$, whereas in W25 and W12.5 the corresponding

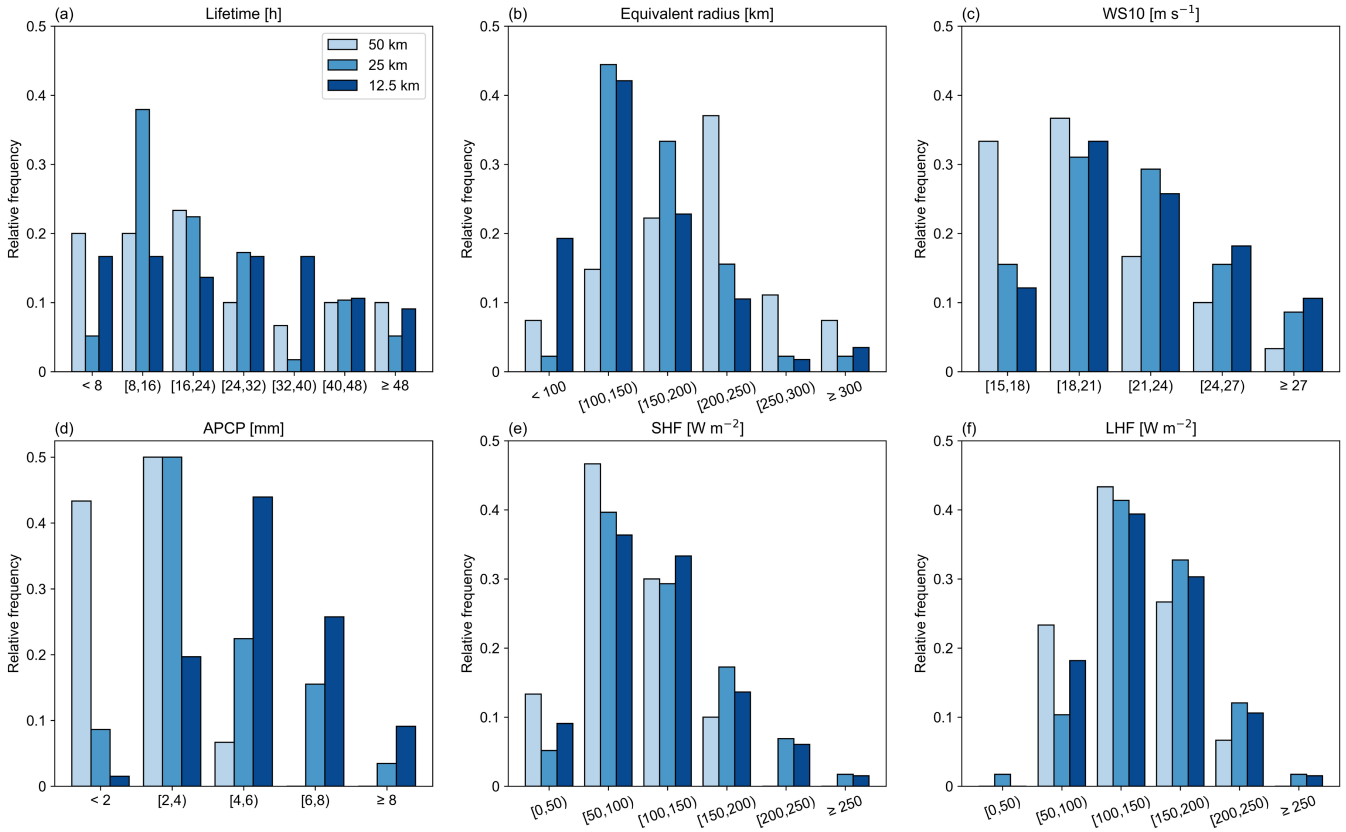

FIGURE 2 | Characteristics of the PLs represented in each simulation: (a) lifetime, (b) average equivalent radius and lifetime maxima of (c) maximum 10-m wind speed, (d) maximum 1-h accumulated precipitation, (e) average surface sensible heat flux and (f) average latent sensible heat flux, all within 200 km of the PL centre.

percentage is 26% and 21%, respectively (Figure 2e). The winter-average of the lifetime maximum of LHF_{avg} is higher in W25 and W12.5 compared to W50 (Figure 2f), but these differences are not statistically significant.

3.2 | Characteristics of PL Tracks Matched Across Simulations

Despite W50 having the fewest PLs, the fraction of PLs that are matched with PLs in the other simulations does not exceed two thirds of those present in W50. In fact, only 10 PLs are matched across all three simulations. When comparing each pair of simulations, we expect that the percentage of PLs in a simulation that have a match in another simulation will increase with the number of PLs present in the latter. This is the case for W25 and W12.5. The percentage of PLs in W25 that match a PL in W50 and W12.5 is, respectively, 33% and 62%. The percentage of PLs in W12.5 that match a PL in W50 and W25 is, respectively, 23% and 55%. However, the percentage of PLs in W50 that match a PL in W25 and W12.5 is, respectively, 63% and 50%.

For each pair of simulations, the lifetimes of some of the matched PLs differ widely, but the average lifetime of the PLs in W50 is similar to that of their counterparts in W25 and W12.5 (Figure S1a,d,g). The average equivalent radius of the PLs in W25 and W12.5 are notably similar, the slope of the least-squares fit to the data being 1 (Figure S1b,e,h). The average equivalent radius of the PLs in W50 are either similar to or larger than those in W25, and W50 can correctly represent some of the smallest PLs. Except for a few cases, the propagation speeds of the matched PLs are rather similar, and the average propagation speeds of the PLs in each simulation are similar to those of their counterparts in the other simulations (Figure S1c,f,i). There is a linear relationship between values in each pair of simulations for $APCP_{max}$, $WS10_{max}$, LHF_{max} and SHF_{max} (Figure 3), which supports that the matched PLs are likely synoptically related to one another. The PLs in the higher-resolution simulations show larger values of the lifetime maximum of $APCP_{max}$ compared to their lower-resolution counterparts. It is particularly noticeable that the values of the lifetime maximum of $APCP_{max}$ are much lower in W50 than in W12.5, the slope of the least-squares fit to the data being 2.6. The lifetime maxima of $WS10_{max}$, SHF_{avg} and LHF_{avg} of the PLs in W25 and W12.5 are larger than those of their respective counterparts in W50. However, the lifetime maxima of $WS10_{max}$, SHF_{avg} and LHF_{avg} of the PLs matched in W25 and W12.5 are similar.

3.3 | Comparison Between Simulated PL Tracks and PL Track Climatologies

Caution must be taken when comparing PL climatologies since the PL tracks obtained depend on the input data, the detection and tracking methodology, the choice of PL criteria and the area and time period covered by the study (Moreno-Ibáñez et al. 2021). The PL tracks of the STARS and Rojo datasets have been obtained using observations—whose temporal resolution and spatial coverage is not high enough to detect all PLs—and the development process has been considered when determining whether a cyclone is a PL. In contrast, the Stoll dataset (Stoll 2022) is based on ERA5—which provides atmospheric fields in a regular grid with high temporal resolution—and the cyclone tracks are not manually analysed to confirm that the PLs are indeed PLs. Therefore, it is reasonable to assume that the STARS and Rojo datasets do not include all occurring PLs, and that the Stoll dataset includes several cyclones that are not really PLs. Accordingly, for the period September 2008 to June 2009, the density of PL tracks in the STARS and Rojo datasets is notably lower than in the Stoll dataset (Figure 1d–f). The number of PL tracks in the STARS and Rojo datasets is, respectively, 30 and 29, and the number of PL tracks in the Stoll dataset is 197. Although some of the PL tracks of the STARS and Rojo datasets are similar, others are only present in one of the two datasets.

For a given dataset, the number of hits increases with the resolution of WRF, and the number of false positives is the lowest for W50, and similar for W25 and W12.5 (Table 4). The hit rate increases with increasing resolution, but the false alarm ratios are rather consistent across resolutions. Therefore, the observed PLs are somewhat better captured as the resolution of the model increases, although the increase in the number of PLs with increasing resolution also leads to a higher number of false positives. In general, the hit rates are low and the false alarm ratios are high for all the simulations. Since the simulations are driven by ERA5 reanalysis, and spectral nudging has been applied, the synoptic-scale patterns represented in the simulation are expected to be similar to the observed ones (Prein et al. 2015). However, the domain of the simulations is large, and mesoscale phenomena may be represented somewhat differently in each simulation.

4 | Conclusion

The objective of this study is to understand the impact of the horizontal resolutions typical of atmospheric climate models on the representation of PLs. Simulations with grid meshes of 50, 25 and 12.5 km were conducted using WRF, and PLs were tracked using a combination of objective and subjective tracking methods. The number of simulated PLs during the winter season 2008–2009 increases as the resolution increases. However, whereas there are twice as many PLs in W25 compared to W50, the increase in the number of PLs is more modest when increasing the resolution from 25 to 12.5 km spacing. A comparison of the simulated PL tracks against three PL climatologies indicates that the skill of the model at capturing observed PLs increases as the resolution increases. The differences in lifetime, propagation speed, distance travelled, minimum SLP and lifetime maximum of LHF_{avg} between each pair of simulations are not statistically significant. However, the PLs in W50 are significantly larger than those in W25 and W12.5, and the lifetime maxima of $WS10_{max}$, $APCP_{max}$ and SHF_{avg} are significantly larger in W25 and W12.5 compared to W50. When comparing W25 and W12.5, the only statistically significant difference found is in the lifetime maximum of $APCP_{max}$, which is larger in the latter. The differences in the characteristics of PLs found when comparing pairs of matched PLs are in line with the differences found when comparing all PL tracks. In summary, a WRF simulation with a grid spacing of 25 km, compared to 50 km, yields smaller, more frequent and more intense PLs, and further increasing the resolution to 12.5 km spacing only leads to an enhancement of

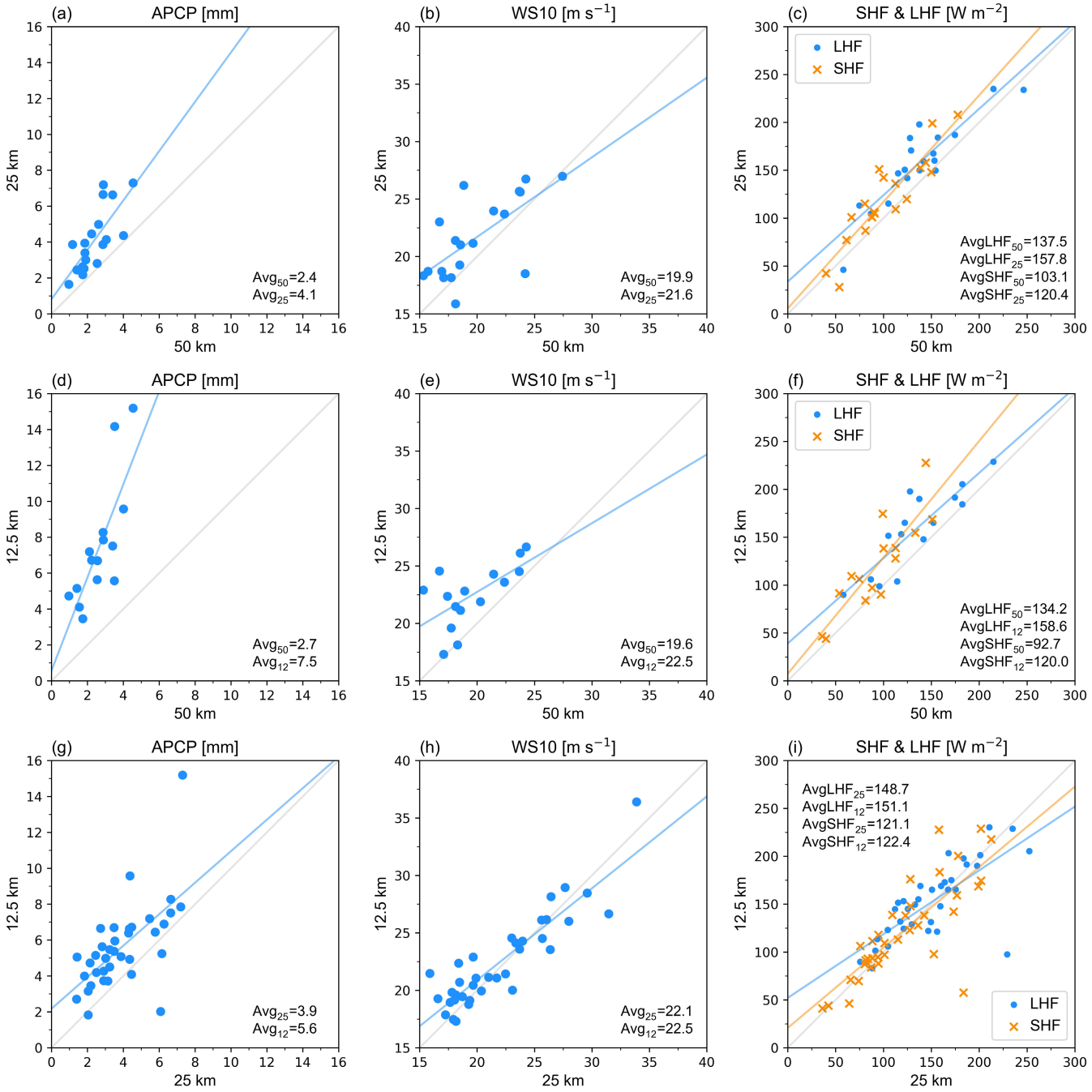

FIGURE 3 | Scatterplots displaying the relationship between the characteristics of the PLs that have been matched across (a–c) W50 and W25, (d–f) W50 and W12.5 and (g–i) W25 and W12.5. For each pair of simulations, the following characteristics of PLs are displayed: Lifetime maxima of the (a, d, g) maximum 1-h accumulated precipitation, (b, e, h) maximum 10-m wind speed and (c, f, i) average surface sensible heat flux and average surface latent heat flux, all within 200 km of the PL centre. The average values of the variables in each simulation are shown. The blue and orange lines represent the least-squares fit to the data, and the grey line is the identity line.

$APCP_{max}$. We conclude that increasing the resolution of atmospheric models from 50 to 25 km will lead to a better representation of PLs and their impact on the ocean in global climate models, but further increasing the resolution to 12.5 km will not lead to a substantial improvement.

This study constitutes a first step in examining how the resolution of an atmospheric model might affect how PLs interact with the ocean. A limitation of this work is the relatively short time period covered, which limits the representativeness in terms of PL characteristics. In addition, given that the accumulated impact of mesoscale SST anomalies over long timescales leads to more intense PLs (Lin et al. 2025), the PLs in the high-resolution simulations may have been more intense if high-resolution ocean surface conditions had been used. Further studies should be done using multiyear simulations with high-resolution coupled atmosphere–ocean–sea ice models. The data needed for such studies could come from the HighResMIP phase 2 (Roberts et al. 2025), which aims to produce global coupled simulations with an atmospheric horizontal grid spacing as high as 10 km.

TABLE 4 | Verification of PL tracks in the WRF simulations against PL climatologies.

	Hit (Miss)			Hit rate		
	50 km	**25 km**	**12.5 km**	**50 km**	**25 km**	**12.5 km**
STARS	4 (26)	8 (22)	10 (20)	0.13	0.27	0.33
Rojo	4 (25)	5 (24)	7 (22)	0.14	0.17	0.24
Stoll	12 (185)	24 (173)	34 (163)	0.06	0.12	0.17
	False positive			**False alarm ratio**		
	50 km	**25 km**	**12.5 km**	**50 km**	**25 km**	**12.5 km**
STARS	24	46	47	0.86	0.85	0.82
Rojo	15	31	29	0.79	0.86	0.81
Stoll	17	32	29	0.59	0.57	0.46

One of the main challenges is to find a suitable automated method to track PLs that can be applied to multiyear simulations since applying a combination of objective and subjective tracking methods, as was done in this study, would not be feasible for such large datasets.

Author Contributions

Marta Moreno-Ibáñez: conceptualization, data curation, formal analysis, funding acquisition, investigation, methodology, software, visualization, writing – review and editing, writing – original draft. **John J. Cassano:** conceptualization, formal analysis, funding acquisition, project administration, methodology, writing – review and editing, supervision. **Suzanne L. Gray:** formal analysis, methodology, supervision, writing – review and editing. **Mark Seefeldt:** software, methodology, writing – review and editing.

Acknowledgements

The authors are grateful to Alex Crawford and Elizabeth Cassano for providing help on how to run the cyclone tracking algorithm. The authors would also like to thank two anonymous reviewers for their constructive comments.

Conflicts of Interest

The authors declare no conflicts of interest.

Data Availability Statement

Data supporting the results reported in this paper are openly available from the University of Reading Research Data Archive at https://doi.org/10.17864/1947.001433 (Moreno-Ibáñez 2025). WRF is available at https://doi.org/10.5065/D6MK6B4K. ERA5 reanalysis, produced by the European Centre for Medium-Range Weather Forecasts, is available through the National Center for Atmospheric Research, Research Data Archive (https://rda.ucar.edu/datasets/ds633.0/) and through Copernicus Climate Change Service Climate Data Store (https://doi.org/10.24381/cds.adbb2d47). The Clouds and the Earth's Radiant Energy System Energy Balanced and Filled TOA and surface monthly means dataset is provided by NASA/LARC/SD/ASDC (2019) (https://doi.org/10.5067/TERRA-AQUA/CERES/EBAF_L3B.004.1). The Equal-Area Scalable Earth 2 grid is provided by the National Snow and Ice Data Center at https://nsidc.org/data/nsidc-0772/versions/1. The STARS dataset is available at https://projects.met.no/stars/data/v3/, the doi of the Rojo dataset is 10.1594/PANGAEA.903058 and the doi of the Stoll dataset is 10.18710/TVZDBF. The doi of the cyclone tracking algorithm (Crawford et al. 2021) code is 10.5281/zenodo.4356161.

References

Blechschmidt, A. M. 2008. "A 2-Year Climatology of Polar Low Events Over the Nordic Seas From Satellite Remote Sensing." *Geophysical Research Letters* 35: L09815. https://doi.org/10.1029/2008GL033706.

Bracegirdle, T. J., and S. L. Gray. 2008. "An Objective Climatology of the Dynamical Forcing of Polar Lows in the Nordic Seas." *International Journal of Climatology* 28: 1903–1919. https://doi.org/10.1002/joc.1686.

Bresson, H., K. I. Hodges, L. C. Shaffrey, G. Zappa, and R. Schiemann. 2022. "The Response of Northern Hemisphere Polar Lows to Climate Change in a 25 Km High-Resolution Global Climate Model." *Journal of Geophysical Research: Atmospheres* 127: e2021JD035610. https://doi.org/10.1029/2021JD035610.

Bromwich, D. H., J. G. Powers, K. W. Manning, and X. Zou. 2022. "Antarctic Data Impact Experiments With Polar WRF During the YOPP-SH Summer Special Observing Period." *Quarterly Journal of the Royal Meteorological Society* 148: 2194–2218. https://doi.org/10.1002/qj.4298.

Cassano, J. J., A. DuVivier, A. Roberts, et al. 2017. "Development of the Regional Arctic System Model (RASM): Near-Surface Atmospheric Climate Sensitivity." *Journal of Climate* 30: 5729–5753. https://doi.org/10.1175/jcli-d-15-0775.1.

Cassano, J. J., M. E. Higgins, and M. W. Seefeldt. 2011. "Performance of the Weather Research and Forecasting Model for Month-Long Pan-Arctic Simulations." *Monthly Weather Review* 139: 3469–3488. https://doi.org/10.1175/MWR-D-10-05065.1.

Chen, F., and J. Dudhia. 2001. "Coupling an Advanced Land Surface–Hydrology Model With the Penn State–NCAR MM5 Modeling System. Part I: Model Implementation and Sensitivity." *Monthly Weather Review* 129: 569–585. https://doi.org/10.1175/1520-0493(2001)129%3C0569:CAALSH%3E2.0.CO;2.

Condron, A., G. R. Bigg, and I. A. Renfrew. 2008. "Modeling the Impact of Polar Mesocyclones on Ocean Circulation." *Journal of Geophysical Research: Oceans* 113: 2007JC004599. https://doi.org/10.1029/2007JC004599.

Condron, A., and I. A. Renfrew. 2013. "The Impact of Polar Mesoscale Storms on Northeast Atlantic Ocean Circulation." *Nature Geoscience* 6: 34–37. https://doi.org/10.1038/ngeo1661.

Crawford, A. D., E. A. P. Schreiber, N. Sommer, et al. 2021. "Sensitivity of Northern Hemisphere Cyclone Detection and Tracking Results to

Fine Spatial and Temporal Resolution Using ERA5." *Monthly Weather Review* 149: 2581–2598. https://doi.org/10.1175/mwr-d-20-0417.1.

Field, P. R., R. Brož ková, M. Chen, et al. 2017. "Exploring the Convective Grey Zone With Regional Simulations of a Cold Air Outbreak." *Quarterly Journal of the Royal Meteorological Society* 143: 2537–2555. https://doi.org/10.1002/qj.3105.

Golubkin, P., J. Smirnova, and L. Bobylev. 2021. "Satellite-Derived Spatio-Temporal Distribution and Parameters of North Atlantic Polar Lows for 2015-2017." *Atmosphere* 12: 224. https://doi.org/10.3390/atmos12020224.

Grell, G. A., and S. R. Freitas. 2014. "A Scale and Aerosol Aware Stochastic Convective Parameterization for Weather and Air Quality Modeling." *Atmospheric Chemistry and Physics* 14: 5233–5250. https://doi.org/10.5194/acp-14-5233-2014.

Gutjahr, O., and C. Mehlmann. 2024. "Polar Lows and Their Effects on Sea Ice and the Upper Ocean in the Iceland, Greenland, and Labrador Seas." *Journal of Geophysical Research: Oceans* 129: e2023JC020258. https://doi.org/10.1029/2023JC020258.

Haarsma, R. J., M. J. Roberts, P. L. Vidale, et al. 2016. "High Resolution Model Intercomparison Project (HighResMIP v1.0) for CMIP6." *Geoscientific Model Development* 9: 4185–4208. https://doi.org/10.5194/gmd-9-4185-2016.

Heinemann, G., and C. Claud. 1997. "Report of a Workshop on "Theoretical and Observational Studies of Polar Lows" of the European Geophysical Society Polar Lows Working Group." *Bulletin of the American Meteorological Society* 78: 2643–2658. https://doi.org/10.1175/1520-0477-78.11.2643.

Hersbach, H., B. Bell, P. Berrisford, et al. 2020. "The ERA5 Global Reanalysis." *Quarterly Journal of the Royal Meteorological Society* 146: 1999–2049. https://doi.org/10.1002/qj.3803.

Hines, K. M., D. H. Bromwich, L. Bai, C. M. Bitz, J. G. Powers, and K. W. Manning. 2015. "Sea Ice Enhancements to Polar WRF." *Monthly Weather Review* 143: 2363–2385. https://doi.org/10.1175/MWR-D-14-00344.1.

Holdsworth, A. M., and P. G. Myers. 2015. "The Influence of High-Frequency Atmospheric Forcing on the Circulation and Deep Convection of the Labrador Sea." *Journal of Climate* 28: 4980–4996. https://doi.org/10.1175/jcli-d-14-00564.1.

Iacono, M. J., J. S. Delamere, E. J. Mlawer, M. W. Shephard, S. A. Clough, and W. D. Collins. 2008. "Radiative Forcing by Long-Lived Greenhouse Gases: Calculations With the AER Radiative Transfer Models." *Journal of Geophysical Research: Atmospheres* 113: 2008JD009944. https://doi.org/10.1029/2008JD009944.

Jung, T., S. Serrar, and Q. Wang. 2014. "The Oceanic Response to Mesoscale Atmospheric Forcing." *Geophysical Research Letters* 41: 1255–1260. https://doi.org/10.1002/2013GL059040.

Kain, J. S. 2004. "The Kain–Fritsch Convective Parameterization: An Update." *Journal of Applied Meteorology* 43: 170–181. https://doi.org/10.1175/1520-0450(2004)043%3C0170:TKCPAU%3E2.0.CO;2.

Kato, S., F. G. Rose, D. A. Rutan, et al. 2018. "Surface Irradiances of Edition 4.0 Clouds and the Earth's Radiant Energy System (CERES) Energy Balanced and Filled (EBAF) Data Product." *Journal of Climate* 31: 4501–4527. https://doi.org/10.1175/JCLI-D-17-0523.1.

Landgren, O. A., Y. Batrak, J. E. Haugen, E. Støylen, and T. Iversen. 2019. "Polar Low Variability and Future Projections for the Nordic and Barents Seas." *Quarterly Journal of the Royal Meteorological Society* 145: 3116–3128. https://doi.org/10.1002/qj.3608.

Lin, T., A. Rutgersson, and L. Wu. 2025. "Influence of Mesoscale Sea Surface Temperature Anomaly on Polar Lows." *Environmental Research Letters* 20: 014051. https://doi.org/10.1088/1748-9326/ad9ec6.

Loeb, N. G., D. R. Doelling, H. Wang, et al. 2018. "Clouds and the Earth's Radiant Energy System (CERES) Energy Balanced and Filled (EBAF) Top-of-Atmosphere (TOA) Edition-4.0 Data Product." *Journal of Climate* 31: 895–918. https://doi.org/10.1175/JCLI-D-17-0208.1.

McInnes, H., J. Kristiansen, J. E. Kristjánsson, and H. Schyberg. 2011. "The Role of Horizontal Resolution for Polar Low Simulations." *Quarterly Journal of the Royal Meteorological Society* 137: 1674–1687. https://doi.org/10.1002/qj.849.

Moreno-Ibáñez, M. 2024. "Polar Low Research: Recent Developments and Promising Courses of Research." *Frontiers in Earth Science* 12: 1368179. https://doi.org/10.3389/feart.2024.1368179.

Moreno-Ibáñez, M. 2025. *North Atlantic Polar Low Tracks From September 2008 to May 2009 From WRF Simulations at 50, 25 and 12.5 km Grid Spacings*. University of Reading. https://doi.org/10.17864/1947.001433.

Moreno-Ibáñez, M., R. Laprise, and P. Gachon. 2021. "Recent Advances in Polar Low Research: Current Knowledge, Challenges and Future Perspectives." *Tellus A* 73: 1–31. https://doi.org/10.1080/16000870.2021.1890412.

Morrison, H., G. Thompson, and V. Tatarskii. 2009. "Impact of Cloud Microphysics on the Development of Trailing Stratiform Precipitation in a Simulated Squall Line: Comparison of One- and Two-Moment Schemes." *Monthly Weather Review* 137: 991–1007. https://doi.org/10.1175/2008MWR2556.1.

Nakanishi, M., and H. Niino. 2006. "An Improved Mellor–Yamada Level-3 Model: Its Numerical Stability and Application to a Regional Prediction of Advection Fog." *Boundary-Layer Meteorology* 119: 397–407. https://doi.org/10.1007/s10546-005-9030-8.

Nakanishi, M., and H. Niino. 2009. "Development of an Improved Turbulence Closure Model for the Atmospheric Boundary Layer." *Journal of the Meteorological Society of Japan. Ser. II* 87: 895–912. https://doi.org/10.2151/jmsj.87.895.

NASA/LARC/SD/ASDC. 2019. *CERES Energy Balanced and Filled (EBAF) TOA and Surface Monthly Means Data in netCDF Edition 4.1*. NASA/LARC/SD/ASDC. https://doi.org/10.5067/TERRA-AQUA/CERES/EBAF_L3B.004.1.

Noer, G., Ø. Saetra, T. Lien, and Y. Gusdal. 2011. "A Climatological Study of Polar Lows in the Nordic Seas." *Quarterly Journal of the Royal Meteorological Society* 137: 1762–1772. https://doi.org/10.1002/qj.846.

Powers, J. G., J. B. Klemp, W. C. Skamarock, et al. 2017. "The Weather Research and Forecasting Model: Overview, System Efforts, and Future Directions." *Bulletin of the American Meteorological Society* 98: 1717–1738. https://doi.org/10.1175/BAMS-D-15-00308.1.

Prein, A. F., W. Langhans, G. Fosser, et al. 2015. "A Review on Regional Convection-Permitting Climate Modeling: Demonstrations, Prospects, and Challenges." *Reviews of Geophysics* 53: 323–361. https://doi.org/10.1002/2014RG000475.

Renfrew, I. A. 2015. "Polar Lows." In *Encyclopedia of Atmospheric Sciences*, edited by G. R. North, J. Pyle, and F. Zhang, 2nd ed., 379–385. Academic Press.

Roberts, M. J., K. A. Reed, Q. Bao, et al. 2025. "High-Resolution Model Intercomparison Project Phase 2 (HighResMIP2) Towards CMIP7." *Geoscientific Model Development* 18: 1307–1332. https://doi.org/10.5194/gmd-18-1307-2025.

Rojo, M., C. Claud, P.-E. Mallet, G. Noer, A. M. Carleton, and M. Vicomte. 2015. "Polar Low Tracks Over the Nordic Seas: A 14-Winter Climatic Analysis." *Tellus A: Dynamic Meteorology and Oceanography* 67: 24660. https://doi.org/10.3402/tellusa.v67.24660.

Rojo, M., C. Claud, G. Noer, and A. M. Carleton. 2019. "In Situ Measurements of Surface Winds, Waves, and Sea State in Polar Lows Over the North Atlantic." *Journal of Geophysical Research – Atmospheres* 124: 700–718. https://doi.org/10.1029/2017JD028079.

Romero, R., and K. Emanuel. 2017. "Climate Change and Hurricane-Like Extratropical Cyclones: Projections for North Atlantic Polar Lows

and Medicanes Based on CMIP5 Models." *Journal of Climate* 30: 279–299. https://doi.org/10.1175/jcli-d-16-0255.1.

Saetra, Ø., T. Linders, and J. B. Debernard. 2008. "Can Polar Lows Lead to a Warming of the Ocean Surface?" *Tellus A* 60: 141–153. https://doi.org/10.1111/j.1600-0870.2007.00279.x.

Seefeldt, M. W., J. J. Cassano, Y. J. Lee, W. Maslowski, A. P. Craig, and R. Osinski. 2024. "Evaluation of Dynamical Downscaling in a Fully Coupled Regional Earth System Model." *Frontiers in Earth Science* 12: 1392031. https://doi.org/10.3389/feart.2024.1392031.

Shkolnik, I. M., and S. V. Efimov. 2013. "Cyclonic Activity in High Latitudes as Simulated by a Regional Atmospheric Climate Model: Added Value and Uncertainties." *Environmental Research Letters* 8: 045007. https://doi.org/10.1088/1748-9326/8/4/045007.

Skamarock, W. C., J. B. Klemp, J. Dudhia, et al. 2019. "A Description of the Advanced Research WRF Version 4." Technical Note NCAR/TN-556+STR, NCAR.

Smirnova, J. E., P. A. Golubkin, L. P. Bobylev, E. V. Zabolotskikh, and B. Chapron. 2015. "Polar Low Climatology Over the Nordic and Barents Seas Based on Satellite Passive Microwave Data." *Geophysical Research Letters* 42: 5603–5609. https://doi.org/10.1002/2015GL063865.

Stoll, P. J. 2022. "A Global Climatology of Polar Lows Investigated for Local Differences and Wind-Shear Environments." *Weather and Climate Dynamics* 3: 483–504. https://doi.org/10.5194/wcd-3-483-2022.

Tewari, M., F. Chen, W. Wang, et al. 2004. "Implementation and Verification of the Unified Noah Land Surface Model in the WRF Model." In *20th Conference on Weather Analysis and Forecasting/16th Conference on Numerical Weather Prediction*. American Meteorological Society.

Tomita, H., and R. Tanaka. 2024. "Ocean Surface Warming and Cooling Responses and Feedback Processes Associated With Polar Lows Over the Nordic Seas." *Journal of Geophysical Research: Atmospheres* 129: e2023JD040460. https://doi.org/10.1029/2023JD040460.

Turner, J., E. A. Rasmussen, and A. M. Carleton. 2003. "Introduction." In *Polar Lows: Mesoscale Weather Systems in the Polar Regions*, edited by E. A. Rasmussen and J. Turner, 1–51. Cambridge University Press.

Wu, L. 2021. "Effect of Atmosphere-Wave-Ocean/Ice Interactions on a Polar Low Simulation Over the Barents Sea." *Atmospheric Research* 248: 105183. https://doi.org/10.1016/j.atmosres.2020.105183.

Wu, L., J. E. Martin, and G. W. Petty. 2011. "Piecewise Potential Vorticity Diagnosis of the Development of a Polar Low Over the Sea of Japan." *Tellus A* 63: 198–211. https://doi.org/10.1111/j.1600-0870.2011.00511.x.

Zahn, M., and H. von Storch. 2010. "Decreased Frequency of North Atlantic Polar Lows Associated With Future Climate Warming." *Nature* 467: 309–312. https://doi.org/10.1038/nature09388.

Zhang, C., and Y. Wang. 2017. "Projected Future Changes of Tropical Cyclone Activity Over the Western North and South Pacific in a 20-Km-Mesh Regional Climate Model." *Journal of Climate* 30: 5923–5941. https://doi.org/10.1175/JCLI-D-16-0597.1.

Supporting Information

Additional supporting information can be found online in the Supporting Information section. **Data S1:** Supporting Information.